39. R. Comin *et al.*, http://arxiv.org/abs/1402.5415 (2014).
40. E. Fradkin, S. A. Kivelson, *Nat. Phys.* **8**, 864–866 (2012).
41. J. C. S. Davis, D.-H. Lee, *Proc. Natl. Acad. Sci. U.S.A.* **110**, 17623–17630 (2013).

ACKNOWLEDGMENTS

We thank J. Shin for the wavelength dispersive x-ray (WDX) measurements, S. Saha for the susceptibility measurements, and N. P. Armitage, S. A. Kivelson, P. A. Lee, and A.-M. S. Tremblay for fruitful discussions. Supported by the Canadian Institute for Advanced Research (CIFAR) Global Academy (E.H.d.S.N.); the Canadian Light Source Graduate Student Travel Support Program (R.C.); the Max Planck–University of British Columbia Centre for Quantum Materials, the Killam, Alfred P. Sloan, Alexander von Humboldt, and NSERC's Steacie Memorial Fellowships (A.D.); the Canada Research Chairs Program (A.D. and G.A.S.); and the Natural Sciences and Engineering Research Council of Canada (NSERC), Canada Foundation for Innovation (CFI), and CIFAR Quantum Materials. Work at the University of Maryland was supported by NSF grant DMR 1104256. All of the x-ray experiments were performed at beamline REIXS of the Canadian Light Source, which is funded by CFI, NSERC, National Research Council Canada, Canadian Institutes of Health Research, the Government of Saskatchewan, Western Economic Diversification Canada, and the University of Saskatchewan.

SUPPLEMENTARY MATERIALS

www.sciencemag.org/content/347/6219/282/suppl/DC1
Materials and Methods
Supplementary Text
Figs. S1 to S4
Reference (*42*)

22 May 2014; accepted 5 December 2014
10.1126/science.1256441

APPLIED PHYSICS

Semiconductor double quantum dot micromaser

Y.-Y. Liu,[1] J. Stehlik,[1] C. Eichler,[1] M. J. Gullans,[2] J. M. Taylor,[2,3] J. R. Petta[1,4]*

The coherent generation of light, from masers to lasers, relies upon the specific structure of the individual emitters that lead to gain. Devices operating as lasers in the few-emitter limit provide opportunities for understanding quantum coherent phenomena, from terahertz sources to quantum communication. Here we demonstrate a maser that is driven by single-electron tunneling events. Semiconductor double quantum dots (DQDs) serve as a gain medium and are placed inside a high-quality factor microwave cavity. We verify maser action by comparing the statistics of the emitted microwave field above and below the maser threshold.

A conventional laser uses an ensemble of atoms that are pumped into the excited state to achieve population inversion (*1*, *2*). Enabled by advances in semiconductor device technology, semiconductor lasers quickly evolved from p-i-n junctions (*3*, *4*), to quantum well structures (*5*) and quantum cascade lasers (QCLs) (*6*). In QCLs, an electrical bias is applied across exquisitely engineered multiple quantum well structures, resulting in cascaded intraband transitions between confined two-dimensional electronic states that lead to photon emission (*7*). However, QCL emission frequencies are set by heterostructure growth profiles and cannot be easily tuned in situ. At the same time, in atomic physics, researchers demonstrated a single-atom maser, where atoms prepared in the excited state transit through a microwave cavity for a precisely controlled period of time, such that the atom "swaps" its excitation to the microwave cavity, generating a large photon field (*8*). These early experiments were extended to a single atom trapped in a high-finesse optical cavity (*9*), as well as condensed-matter systems, where artificial atoms were strongly coupled to cavities (*10*–*14*).

Here we demonstrate a maser that is driven by single-electron tunneling events. The gain medium consists of semiconductor double quantum dots (DQDs) that support zero-dimensional electronic states (*15*). Electronic tunneling through the DQDs generates photons that are coupled to a cavity mode (*16*). In contrast to optically pumped systems, population inversion is generated in the DQD system through the application of a bias voltage that results in sequential single-electron tunneling.

The maser consists of two semiconductor DQDs (referred to as the left DQD and right DQD, Fig. 1), which are electric-dipole coupled to a microwave cavity. The cavity is formed from a half-wavelength ($\lambda/2$) superconducting Nb transmission line resonator with a center frequency f_c = 7880.55 MHz and a loaded quality factor $Q_c \approx 3000$ (*17*, *18*). Two lithographically defined InAs nanowire DQDs serve as the maser gain medium (*16*, *19*). Each DQD is fabricated by placing a single InAs nanowire over five Ti/Au bottom gate electrodes (Fig. 1C) (*20*, *21*). The bottom gates create a tunable DQD confinement potential in the nanowire (*21*). Electrostatically defined DQDs, often regarded as artificial molecules (*15*), are a unique gain medium. They are fully reconfigurable, with electronic transitions that can be tuned from gigahertz to terahertz frequencies.

A source-drain bias voltage V_{SD} = 2 mV is applied across the DQDs to drive a current. The energy levels of each DQD can be separately tuned and are described by the left (right) DQD detuning ε_L (ε_R). Current will flow in a nanowire DQD through a series of downhill (in energy) single-electron tunneling events (see level diagrams in Fig. 1B). In contrast with quantum well structures, current results from single-electron tunneling events between electrically tunable zero-dimensional states in the DQD (*15*, *22*). Electron tunneling results in microwave gain, which is accessed by measuring the transmission through the cavity (*16*).

To measure the gain, the cavity is driven with a coherent field at frequency $f_{in} = f_c$ with a power P_{in}. Measurements of the output power P_{out} yield the power gain $G = CP_{out}/P_{in}$, where C is a normalization constant set such that G = 1 when both DQDs are in Coulomb blockade (no current flow) (*16*, *23*). With V_{SD} = 0, charge dynamics within the DQD result in an effective microwave admittance that damps the electromagnetic field inside the cavity, yielding $G < 1$ (*18*, *24*, *25*). Application of a source-drain bias that drives sequential tunneling through the DQD can lead to gain in the cavity transmission, $G > 1$ (*16*). In Fig. 1D, we plot G as a function of ε_L for V_{SD} = 2 mV and $f_{in} = f_c$. For downhill electron tunneling ($\varepsilon_L > 0$), we measure a maximum gain $G \approx 7$ (*23*). In contrast, for $\varepsilon_L < 0$, the left DQD can absorb a photon from the cavity, leading to loss $G \approx 0.2$ (*18*, *25*). These data are acquired with the right DQD configured in Coulomb blockade such that the current is zero (*15*). For simplicity, we refer to a DQD as "on" when its detuning is set to achieve maximum gain and "off" when the DQD is configured in Coulomb blockade with G = 1.

We investigate the cavity response by measuring G as a function of f_{in} with P_{in} = −120 dBm (Fig. 2). The black curve is the "cold cavity transmission" obtained with both DQDs configured in the off state, where the maximum G = 1. Here the gain curve is a Lorentzian with a width set by the cavity decay rate $\kappa/2\pi$ = 2.6 MHz. When ε_L is set to the gain peak shown in Fig. 1D, we observe a maximum $G \approx 16$ at f_{in} = 7880.30 MHz. Similarly, with the right DQD on and the left DQD off, we observe a maximum $G \approx 6$ at f_{in} = 7880.41 MHz. In both configurations, the observed gain rate is too small to reach the maser threshold. In contrast, the red curve in Fig. 2 shows the gain curve with both DQDs in the on state. Here the cavity response is sharply peaked at f_{in} = 7880.25 MHz, yielding a maximum gain $G \approx 1000$, which is much larger than the product of the individual gains.

We next examine the characteristics of the device in free-running mode (with no cavity drive tone). Figure 3 shows the power spectral density $S(f)$ of microwave radiation emitted from the cavity in the on/on configuration. The spectrum is

[1]Department of Physics, Princeton University, Princeton, NJ 08544, USA. [2]Joint Quantum Institute, University of Maryland–National Institute of Standards and Technology, College Park, MD 20742, USA. [3]Joint Center for Quantum Information and Computer Science, University of Maryland and NIST, College Park, MD 20742, USA. [4]Department of Physics, University of California, Santa Barbara, CA 93106, USA.
*Corresponding author. E-mail: petta@princeton.edu

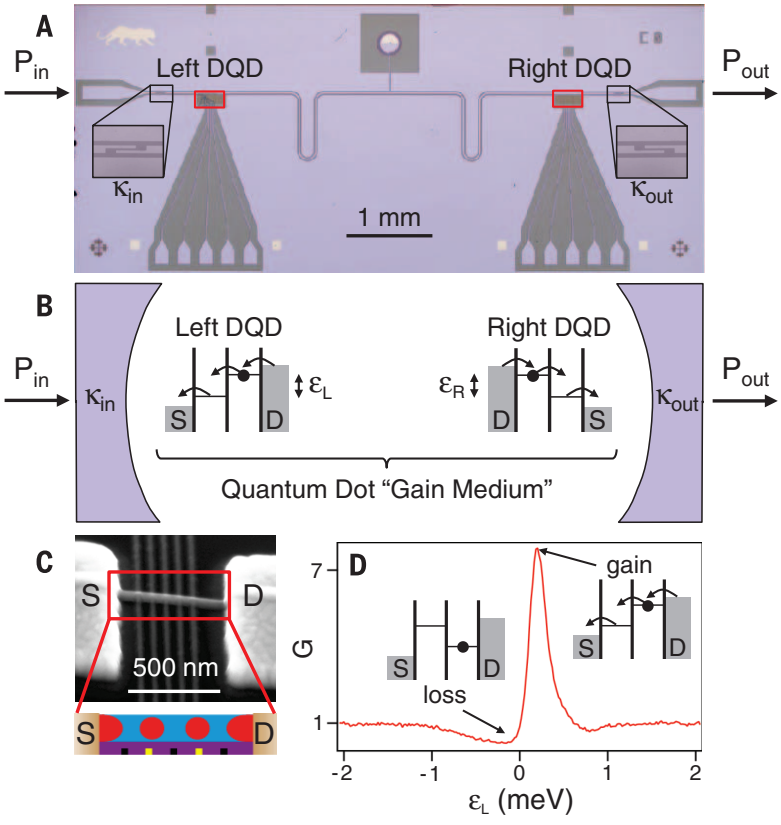

Fig. 1. Double quantum dot micromaser. (**A**) Optical micrograph of the DQD micromaser. Cavity photons are coupled to input and output ports with rates κ_{in} and κ_{out}. (**B**) Schematic illustration of the DQD micromaser. Two DQDs are electric-dipole coupled to the microwave cavity. Single-electron tunneling through the DQDs leads to photon emission into the cavity mode. Left (right) DQD detunings ε_L (ε_R) are independently tunable. (**C**) Scanning electron microscope image of an InAs nanowire DQD. (**D**) G as a function of ε_L (measured at frequency f_c) with V_{SD} = 2 mV and the right DQD configured in Coulomb blockade. Insets: For $\varepsilon_L > 0$, electron transport proceeds downhill in energy, resulting in a gain exceeding 7. With $\varepsilon_L < 0$, an electron will be trapped in the right dot until a photon is absorbed, resulting in cavity loss, $G < 1$.

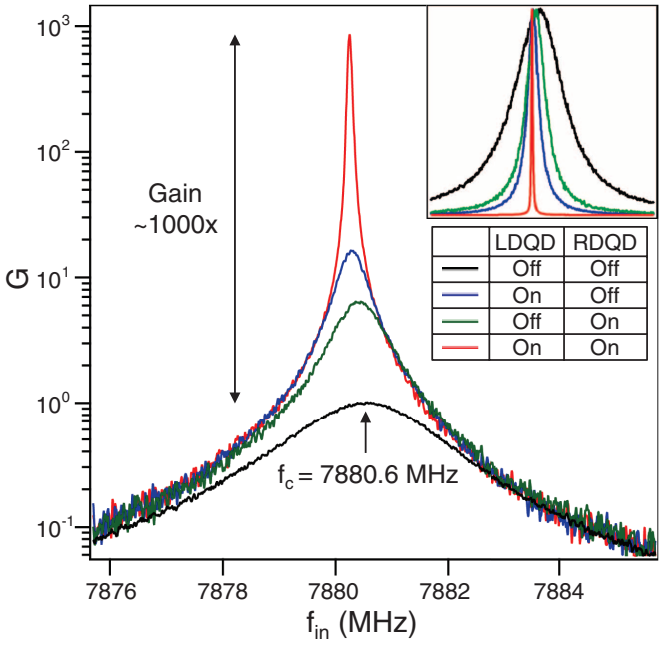

Fig. 2. Microwave gain induced by single-electron tunneling. G as a function of f_{in} with P_{in} = –120 dBm. The black curve is obtained with both DQDs in Coulomb blockade (in the off/off state). With the left DQD set at a detuning that results in gain (see Fig. 1D) and the right DQD in Coulomb blockade (on/off state), we measure a maximum $G \approx 16$. Similarly, in the off/on state, we observe a gain of ≈ 6. Maser action occurs when both DQDs are tuned to produce gain, resulting in $G \approx 1000$. (**Inset**) Data plotted on a linear scale and normalized to the same height.

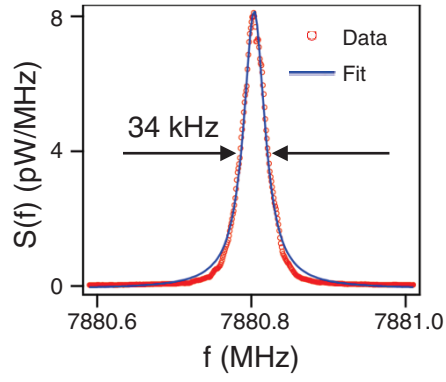

Fig. 3. Maser coherence time. Power spectral density $S(f)$ measured in free-running maser mode (on/on state with no cavity drive applied). The maser emission peak width Δ_f = 34 kHz (FWHM) yields a coherence length l_{coh} = 2.8 km.

sharply peaked around f = 7880.8 MHz and has a full-width at half-maximum (FWHM) Δ_f = 34 kHz, which corresponds to a coherence time $\tau_{coh} = 1/\pi\Delta_f = 9.4$ μs and a coherence length $l_{coh} = \tau_{coh}c = 2.8$ km, where c is the speed of light. The measured linewidth is roughly a factor of 100 larger than the Schawlow-Townes prediction, but it is not uncommon for conventional semiconductor lasers to have broad emission linewidths (*23*, *26*, *27*). Time domain measurements of τ_{coh} are shown in (*23*).

The most notable evidence of above-threshold maser action is obtained by comparing the statistics of the radiation emitted from the device in the off/on and on/on configurations (*23*). For this purpose, we have sampled the voltages of the down-converted cavity output field to heterodyne detect the in-phase and quadrature phase components I and Q with a rate of 1 MHz

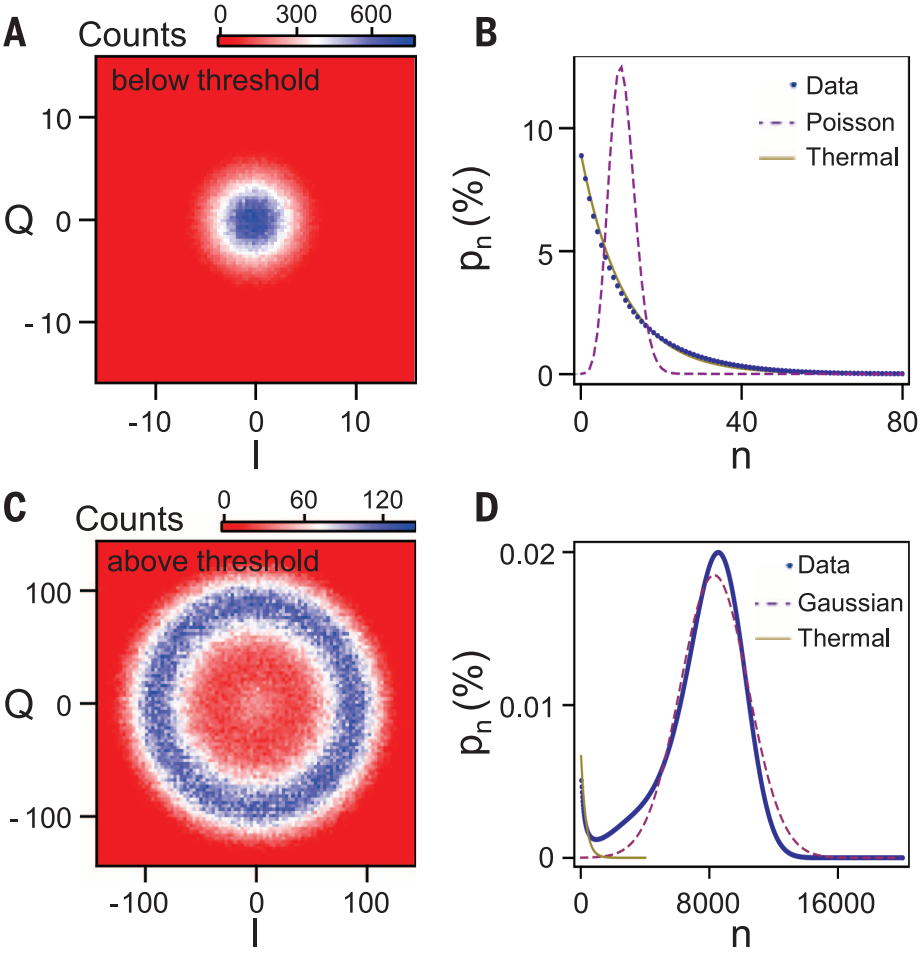

Fig. 4. Photon statistics. (**A**) *IQ* histogram acquired below threshold (off/on configuration). (**B**) The photon number distribution, p_n, extracted from the data in (A) is consistent with a thermal distribution (solid line). A Poisson distribution (dashed line) with $\overline{N}$ = 11.4 is shown for comparison. (**C**) *IQ* histogram measured above threshold (on/on configuration). Here the extracted photon number distribution (**D**) is peaked around n = 8000 and is compared with a Gaussian distribution (dashed line). A small thermal component (solid line) is attributed to charge fluctuations, which shift the device below threshold.

after applying a 1-MHz digital filter. We store 4×10^5 individual (I,Q) measurements in two-dimensional histograms $D(I,Q)$ to analyze their statistical properties. The measured *IQ* histogram for the off/on configuration (Fig. 4A) is centered near the origin, and the extracted photon number distribution (Fig. 4B) is consistent with a thermal source (*23*). In contrast, Fig. 4C shows the *IQ* histogram for the on/on configuration. Here the *IQ* histogram has a donut shape, consistent with an above-threshold maser (*2*). The extracted photon number distribution is peaked around a photon number n = 8000, giving strong evidence for above-threshold behavior. The peak in the photon number distribution is well fit with a Gaussian lineshape, but its width is considerably larger than that of an ideal coherent state $\sqrt{\overline{N}} \approx 90$, where $\overline{N}$ is the average photon number (*23*). Time domain measurements of the maser emission indicate that charge noise fluctuations, which shift the detuning of the DQD gain medium, are most likely responsible for the broadening. Charge noise also occasionally shifts the system below threshold, leading to the small thermal component observed in Fig. 4D (*23*).

We have demonstrated a maser whose gain medium consists of electrically tunable semiconductor DQDs. Single-electron tunneling in the DQDs provides the energy source for maser action, and a maximum power gain of 1000 is observed. Above-threshold maser action is verified by measuring the statistics of the emitted photon field. Through further improvements in the cavity quality factor (*28*), it may be possible to exceed the lasing threshold with a single DQD emitter. In this case, theory predicts "thresholdless lasing" (*29*). Lastly, the large single-particle level spacings allow for an operation frequency that is purely set by the cavity resonance frequency. This will enable maser operation across a very wide frequency range, spanning gigagertz to terahertz frequencies, a feature that is specific to gate-defined quantum dots, where electron tunneling takes place between confined zero-dimensional electronic states.

REFERENCES AND NOTES

1. H. Haken, *Laser Theory* (Springer, Berlin, 1983).
2. A. E. Siegman, *Lasers*. (University Science Books, Mill Valley, CA, 1986).
3. R. N. Hall, G. E. Fenner, J. D. Kingsley, T. J. Soltys, R. O. Carlson, *Phys. Rev. Lett.* **9**, 366–368 (1962).
4. M. I. Nathan, W. P. Dumke, G. Burns, F. H. Dill, G. Lasher, *Appl. Phys. Lett.* **1**, 62–64 (1962).
5. R. Dingle, W. Wiegmann, C. H. Henry, *Phys. Rev. Lett.* **33**, 827–830 (1974).
6. J. Faist *et al*., *Science* **264**, 553–556 (1994).
7. Y. Yao, A. J. Hoffman, C. F. Gmachl, *Nat. Photonics* **6**, 432–439 (2012).
8. D. Meschede, H. Walther, G. Müller, *Phys. Rev. Lett.* **54**, 551–554 (1985).
9. J. McKeever, A. Boca, A. D. Boozer, J. R. Buck, H. J. Kimble, *Nature* **425**, 268–271 (2003).
10. T. Yoshie *et al*., *Nature* **432**, 200–203 (2004).
11. J. P. Reithmaier *et al*., *Nature* **432**, 197–200 (2004).
12. Z. G. Xie, S. Götzinger, W. Fang, H. Cao, G. S. Solomon, *Phys. Rev. Lett.* **98**, 117401 (2007).
13. M. Nomura, N. Kumagai, S. Iwamoto, Y. Ota, Y. Arakawa, *Nat. Phys.* **6**, 279–283 (2010).
14. O. Astafiev *et al*., *Nature* **449**, 588–590 (2007).
15. W. G. van der Wiel *et al*., *Rev. Mod. Phys.* **75**, 1–22 (2002).
16. Y.-Y. Liu, K. D. Petersson, J. Stehlik, J. M. Taylor, J. R. Petta, *Phys. Rev. Lett.* **113**, 036801 (2014).
17. A. Wallraff *et al*., *Nature* **431**, 162–167 (2004).
18. T. Frey *et al*., *Phys. Rev. Lett.* **108**, 046807 (2012).
19. P.-Q. Jin, M. Marthaler, J. H. Cole, A. Shnirman, G. Schön, *Phys. Rev. B* **84**, 035322 (2011).
20. C. Fasth, A. Fuhrer, L. Samuelson, V. N. Golovach, D. Loss, *Phys. Rev. Lett.* **98**, 266801 (2007).
21. S. Nadj-Perge, S. M. Frolov, E. P. A. M. Bakkers, L. P. Kouwenhoven, *Nature* **468**, 1084–1087 (2010).
22. R. Hanson, L. P. Kouwenhoven, J. R. Petta, S. Tarucha, L. M. K. Vandersypen, *Rev. Mod. Phys.* **79**, 1217–1265 (2007).
23. Supplementary materials are available on *Science* Online.
24. M. R. Delbecq *et al*., *Phys. Rev. Lett.* **107**, 256804 (2011).
25. K. D. Petersson *et al*., *Nature* **490**, 380–383 (2012).
26. A. L. Schawlow, C. H. Townes, *Phys. Rev.* **112**, 1940–1949 (1958).
27. P. W. Milonni, J. H. Eberly, *Laser Physics* (Wiley, Hoboken, NJ, 2010).
28. A. Megrant *et al*., *Appl. Phys. Lett.* **100**, 113510 (2012).
29. I. Protsenko *et al*., *Phys. Rev. A* **59**, 1667–1682 (1999).

ACKNOWLEDGMENTS

We thank K. Petersson for assistance with sample fabrication. Research was supported by the Packard Foundation, National Science Foundation (DMR-1409556 and DMR-1420541), Defense Advanced Research Projects Agency QuEST (HR0011-09-1-0007), and Army Research Office (W911NF-08-1-0189). Identification of certain commercial equipment, instruments, or materials (or suppliers or software) in this paper does not imply recommendation or endorsement by the National Institute of Standards and Technology, nor does it imply that the materials or equipment identified are necessarily the best available for the purpose. All data described in the paper are presented in this report and supplementary materials. Y.-Y.L., J.R.P., and Princeton University have filed a provisional patent application that relates to the quantum dot micromaser.

SUPPLEMENTARY MATERIALS

www.sciencemag.org/content/347/6219/285/suppl/DC1
Materials and Methods
Supplementary Text
Figs. S1 to S6
References (*30*–*39*)

7 November 2014; accepted 12 December 2014
10.1126/science.aaa2501

Semiconductor double quantum dot micromaser

Y.-Y. Liu, J. Stehlik, C. Eichler, M. J. Gullans, J. M. Taylor and J. R. Petta

Science **347** (6219), 285-287.
DOI: 10.1126/science.aaa2501

Tunnel through and emit coherently

The generation of coherent light (lasers and masers) forms the basis of a large optics industry. Liu *et al.* demonstrate a type of laser that is driven by the tunneling of single electrons in semiconductor double-quantum dots. Distinct from other existing semiconductor lasers, the emission mechanism is driven by tunneling of single charges between discrete energy levels that are electrically tunable. The ability to tune the levels by single-electron charging would allow their laser (or maser) to be turned on and off rapidly.

Science, this issue p. 285